ESTIMATION OF ROTATING RSO PARAMETERS USING RADAR DATA AND JOINT TIME-FREQUENCY TRANSFORMS

S. Ghio [2] **and M. Martorella** [1,2]

[1] *National Laboratory of Radar and Surveillance Systems (RaSS) - CNIT, 56122 Pisa, Italy*

[2] *University of Pisa, Department of Information Engineering, 56122 Pisa, Italy*
Email: {selenia.ghio@ing.unipi.it, marco.martorella@iet.unipi.it}

ABSTRACT

The amount of space debris is increasing faster than expected. This growth represents a serious hazard for operational spacecraft and human activities in space, especially in the Low-Earth Orbit (LEO) . In order to guarantee the safety of outer space activities, space object catalogues must be created and maintained. In this paper, an approach for estimating the geometrical and motion parameters of Resident Space Objects (RSOs) located in the LEO region is proposed by using a radar system. Time-frequency based signal processing is developed to estimate RSO's parameters and therefore support RSOs' classification and data association in Initial Orbit Determination (IOD).

Keywords: feature extraction; resident space object (RSO); inverse Radon transform (IRT); radar; short time Fourier transform (STFT); SSA; SST; space debris.

1. INTRODUCTION

Resident Space Objects (RSOs) are represented by both active satellites and space debris in orbit around the Earth. Space debris are all man-made objects in Earth orbit or re-entering the atmosphere that are non-functional. Scientists have estimated that there are about 20,000 particles of space debris measuring more than 10 cm in diameter hurtling around the Earth at an average velocity of 25,000 km/h ($\sim$ 7 Km/s), not counting the 700,000 or so particles with a diameter between 1 and 10 cm. LEO is the region of space in which the risk of collisions is at its greatest – especially at an altitude of 800 km above Earth [1, 2]. Although small, these items of space debris travel so fast that they could easily damage or destroy an operational satellite. Space collisions can have a closing speed up to 15 km/s and even small particles are a serious safety concern [3]. If a collision occurs, resulting fragments can become an additional collision risk. A chain reaction may occur that pulverizes everything in orbit, including functioning satellites. Knowledge of the changing debris environment is necessary for both space mission design and for the assessment of debris mitigation policies.

Space Surveillance and Tracking (SST) systems are then required to keep track of RSOs to support collision avoidance strategies. One of the main issues in SST is unique data association from one passage to the next [4].

Both optical and radar measurements are used by SST systems. In this paper, we will focus on the latter and provide an object parameter estimation algorithm that is able to improve the object unique identification and consequently the data association, which is one of the key points recommended in [5].

The echo signals generated by rotating objects have spectral contents that change with time (non-stationary signals). The same characteristics are shown in signals generated by micro-Doppler (μD) modulations, as widely demonstrated in the radar literature [6] . Due to lack of localized time information, the widely used Fourier Transform (FT) cannot provide time-varying frequency modulation information. A Joint Time-Frequency Analysis (JTFA) that provides localized time-dependent frequency information is needed for extracting time-varying motion dynamic features. Time-frequency Distributions (TFDs) include linear and bilinear transforms, such as the Short Time Fourier Transform (STFT) and Wigner-Ville distribution (WVD), respectively.

According to the literature several methods have been proposed to extract information about spinning RSO characteristics.

In [7] T. Sato introduced Single-Range Doppler Interferometry (SRDI) to obtain the two-dimensional image of a space debris and thus estimate its shape by using spectrogram characteristics of target's echoes. In [8] and [9] J. Li et al. proposed the Coherent Single-Range Doppler Interfermetry (CSRDI) which could be regarded as a modified method of the SRDI, which utilizes both the magnitude and phase of the time-frequency spectrogram to reconstruct the target's geometry.

In this paper, the STFT is taken into consideration as a tool for the time-frequency localization of such signals.

The proposed method is based on the fact that the TFD of a rotating rigid-body is a sinusoidal signature from which it is possible to extract some geometrical and motion parameters.

RSO's parameters that can be estimated using radar data are: the *rotation period* (T_Ω), the *maximum Doppler frequency* ($f_{D_{max}}$) and the *maximum size of the object projected onto the radar Line Of Sight* (LOS) ($D_\perp$). Those parameters are useful to discriminate among RSOs. In fact, it is likely that two RSOs would be characterized by different values of T_Ω, $f_{D_{max}}$ and $D_\perp$.

In order to extract those parameters from the STFT of the received signal, the inverse Radon Transform (IRT) is considered. In fact, such transform allows for 2-D sinusoidal patterns to be mapped onto a single point (SP) in the IRT domain. When considering rigid bodies, each SP has the same period, therefore, each of such point can be used to estimate the rotation period (T_Ω). Further analysis on each extracted SP can also provide information about $f_{D_{max}}$ and $D_\perp$.

In order to test the proposed method, simulated radar signal returns generated from a data set of objects with different shapes, sizes and angular rates have been used. The simulated data used in this paper is obtained by generating the backscattered signal from 8 different point-like scatterer models. The proposed method has shown good performances for all types of objects considered both in terms of accuracy and robustness against noise.

The organization of this paper is as follows. The received signal model is discussed in Section 2. The object parameters are defined in Section 3. The feature estimation technique is defined in Section 4. The performance analysis of the proposed algorithm is shown in Section 5.

2. RECEIVED SIGNAL MODEL

The received signal model is described in this section, according to the acquisition system geometry.

2.1. Geometry

Let us consider a simple geometry, as shown in Figure 1. The monostatic radar consists of a colocated transmitter and receiver (TX/RX), it is located in the origin of the reference system (X,Y,Z). The Y axis is aligned with the radar LOS.

The radar is stationary and located at the origin Q of the radar-fixed coordinate system (X, Y, Z) as shown in Figure 1. The local reference system (x, y, z) is fixed on the target, which is moving with linear and rotational motions with respect to the radar coordinates. The origin O of the reference system is assumed to be at a distance R_0 from the radar. By considering the target as a rigid body,

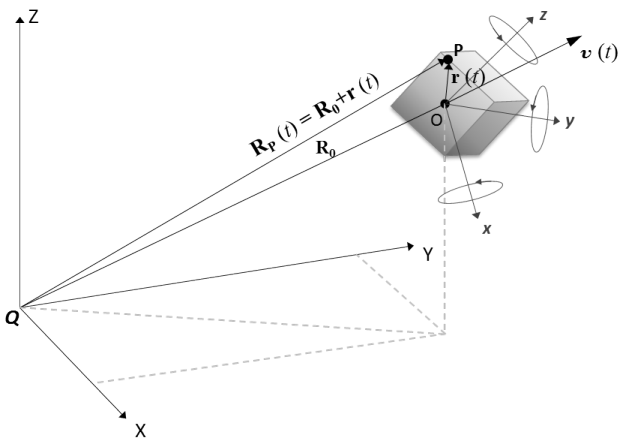

Figure 1: Geometry of the radar and a target with translational and rotational motions

the relative radar target motion can be considered as the superimposition of two contributions: a translational motion and an angular motion, which are applied to the center O of the target. The translational motion is denoted by the *translational rotation vector* $\boldsymbol{v}(t)$. The angular motions are represented by the *angular rotation vector* $\boldsymbol{\omega}(t)$. The sum of these two rotation vectors yields the *total angular rotation vector* $\boldsymbol{\omega}_T(t)$. The projection of $\boldsymbol{\omega}_T(t)$ onto the plane orthogonal to the LOS is the *effective rotation vector* $\boldsymbol{\omega}_{eff}(t)$ and it determines the target aspect angle variation .

In particular, $\boldsymbol{\omega}_{eff}(t)$ can be expressed as:

$$\boldsymbol{\omega}_{eff}(t) = \hat{\mathbf{i}}_{LOS} \times \left(\boldsymbol{\omega}_T(t) \times \hat{\mathbf{i}}_{LOS}\right) \qquad (1)$$

where $\hat{\mathbf{i}}_{LOS}$ is the LOS unit vector in the (X, Y, Z) reference system.

The range from the radar to the scatterer can be defined as $\mathbf{R_P}(t) = \mathbf{R_0} + \mathbf{r}(t)$ where $\mathbf{R_0} = R_0\hat{\mathbf{i}}_{LOS}$ denotes the distance between the radar and the center of rotation O on the target and $\mathbf{r}(t)$ is the distance from a scatterer on the target with respect to O.

2.2. Signal model

Space debris may rotate rapidly around an axis, usually its major axis, such motion is known as spin. In order to introduce a radar signal model for such objects, some assumptions can be made: a) the spinning rate remains constant within the acquisition interval; b) the translational motion is completely compensated ; c) the far-field condition is satisfied. The target can be considered as composed of point-like scatterers corresponding to primary reflecting scatterers. The point scattering model simplifies the analysis while preserving the object geometrical features. In the simplified model, scatterers are assumed to be isotropic reflectors.

When a radar transmits an electromagnetic (EM) wave at a carrier frequency f_0, the received radar signal can be expressed as follows:

$$\begin{aligned} \mathbf{s_R}(t) &= \mathbf{s_T}(t)\, e^{-j4\pi f_0 \mathbf{R_P}(t)} = \\ &= \mathbf{s_T}(t)\, e^{-j\Phi(t)} \end{aligned} \tag{2}$$

where $\Phi(t) = -j4\pi f_0 \mathbf{R_P}(t)$ is the phase function at time t. The modulation induced by rotation structure can be regarded as a unique signature of the target.

The spectrogram ($\mathbf{S}(t,f)$) of $\mathbf{s_R}(t)$ is defined as the squared modulus of its Short-Time Fourier Transform (STFT)

$$\mathbf{S}(t,f) = |\mathbf{STFT}(t,f)|^2 \tag{3}$$

where

$$\mathbf{STFT}(t,f) = \int \mathbf{s_R}(\tau)\, \mathbf{h}(t-\tau)\, e^{-j2\pi f\tau} d\tau \tag{4}$$

and $\mathbf{h}(t)$ is the analysis window. In the discrete domain it becomes

$$\mathbf{S}(n,k) = |\mathbf{STFT}(n,k)|^2 \tag{5}$$

where

$$\mathbf{STFT}(n,k) = \sum_{m=0}^{N_h-1} \mathbf{h}(m)\, \mathbf{s_R}(n+m)\, e^{-j\frac{2\pi}{N_h}mk} \tag{6}$$

and $\mathbf{h}(n)$ is the discrete analysis window of length N_h.

3. OBJECT DYNAMICAL AND GEOMETRICAL PARAMETERS

As already pointed out, the radar back-scattering from rotating objects is subject to Doppler modulations that enable the determination of dynamic properties of objects and provides useful information about them. By observing RSOs using a radar, useful parameters for their discrimination can be identified as T_Ω, $f_{D_{max}}$ and $D_\perp$. In particular, such parameters can split into two categories:

- geometry dependent parameters ($f_{D_{max}}$, $D_\perp$)
- geometry independent parameters (T_Ω)

The former depends on the acquisition geometry whereas the latter does not.

If the target moves with a constant rotational motion, then $\boldsymbol{\omega} = \Omega\hat{\boldsymbol{\omega}}$ where Ω is the amplitude and $\hat{\boldsymbol{\omega}}$ is the unit vector of the vector $\boldsymbol{\omega}$. The instantaneous frequency of the received signal can described as $f_i(t) = 2f_0/c\,[\boldsymbol{\omega} \times \mathbf{r}(t)] \cdot \hat{\mathbf{i}}_{LOS}$.

The amplitude of $f_i(t)$ depends on the LOS direction: in fact, if $\hat{\mathbf{i}}_{LOS}$ and $\hat{\boldsymbol{\omega}}$ are parallel, $f_i(t)$ would be zero despite the target's rotation. The optimal case is when the two vectors are perpendicular to each other since the $f_i(t)$ is maximum and therefore its measurement is facilitated. The spectrogram ($\mathbf{S}(t,f)$) of a rotating rigid-body contains a sinusoid for each scatterer with:

- the same T_Ω and $\Omega = \mid \boldsymbol{\omega} \mid$ (because of the rigidity property)
- different amplitudes f_D depending on their distance from the center of rotation (O)
- different phases according to their position with respect to the radar

Thus, if we estimate one of these sinusoids we can extract the information about T_Ω (and so Ω) of the observed RSO. It is self-evident that the furthest scatterer from O is associated to the signature with the highest amplitude in $\mathbf{S}(t,f)$. By estimating such sinusoid, we obtain also the information about $f_{D_{max}}$. Moreover, if we select the edge signatures, no matter if O is a center of symmetry, it is possible to estimate the maximum projected size of the *Object Under Test* (OUT). It should be pointed out that with the term "*maximum projected size*" we do not refer to the object maximum size, but only to its projection onto the LOS during the *Observation Time* (T_{ob}). The worst scenario occurs if $\hat{\mathbf{i}}_{LOS}$ and $\hat{\boldsymbol{\omega}}$ are parallel, in this case the radar can not measure the rotation of the RSO and it would not be possible to estimate its size. It is important to note that by observing the same object with different acquisition geometries, the actual object maximum size could be inferred.

4. PARAMETER ESTIMATION

The feature extraction algorithm is summarized in Figure 2:

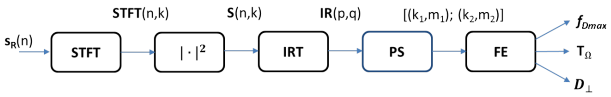

Figure 2: Feature Extraction Algorithm Workflow

More details on the steps for the Peak Selection (PS) are depicted in Figure 3.

The Radon transform of a two-dimensional signal containing a two-dimensional Dirac function is a sinusoidal pattern with amplitude corresponding to the distance of the point from the origin and the initial angle corresponding to the phase of the point position. Therefore, a sinusoidal pattern in the time-frequency plane (produced by a time-frequency representation of sinusoidally modulated signal) is projected onto a two-dimensional point

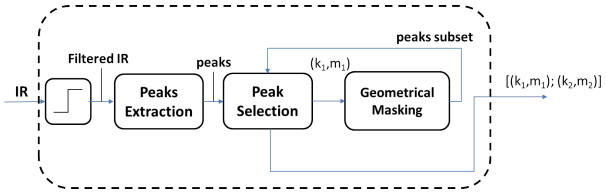

Figure 3: Peak Selection (PS) Workflow

in an Inverse Radon Transform (IRT) [10]. By calculating the IRT on a multi-component sinusoidal signal, the energy of each sinusoid is concentrated into a point. The IRT of $\mathbf{S}(t,f)$ is evaluated for each vector of angles $\boldsymbol{\alpha}(i) = \boldsymbol{\theta}_{set}\mathbf{n}(i)$. The vector $\boldsymbol{\theta}_{set}$ is a vector of L equally spaced values between 0 and 2π and $\mathbf{IR}(p,q)$ is the IRT of the OUT and contains a point for every signature. L represents the column size of $\mathbf{S}(t,f)$. The vector $\mathbf{n}$ contains the possible number of periods of the RSO in T_{ob}, i.e., $\mathbf{n} = [n_1, n_2, ..., n_i, ..., n_l]$. Among all the computed IRT, we pick the one with the highest concentration according to the *Concentration Measure* (M) [11] as defined in Equation 7. This is done because the points in IRT have the highest concentration when the IRT is calculated using the right number of periods contained in the spectrogram .

$$\mathrm{M} = \frac{\sum_p \sum_q \left[\mathbf{IR}(p,q) + |\mathbf{IR}(p,q)|\right]^4}{\left\{\sum_p \sum_q \left[\mathbf{IR}(p,q) + |\mathbf{IR}(p,q)|\right]^2\right\}^2} \tag{7}$$

The *Concentration Measure* (M) calculated in correspondence of the i-th index is as follows:

$$\mathbf{M}_i = \frac{\sum_p \sum_q \left[\mathbf{IR_i}(p,q) + |\mathbf{IR_i}(p,q)|\right]^4}{\left\{\sum_p \sum_q \left[\mathbf{IR}_i(p,q) + |\mathbf{IR}_i(p,q)|\right]^2\right\}^2} \tag{8}$$

where,

$$\mathbf{IR}_i(p,q) = \mathrm{IRT}\left(\mathbf{S}(t,f), \boldsymbol{\theta}_{set}\mathbf{n}(i)\right) \tag{9}$$

High values of $\mathbf{M}$ indicate that the representation is highly concentrated, and vice versa. The optimum value n^{opt} is the one that maximizes $\mathbf{M}$ according to the concentration criterion:

$$n^{opt} = \mathbf{n}(i^{opt}) \tag{10}$$

$$i^{opt} = \arg \max_{\mathbf{i} \in [1,2,...,\mathrm{I}]} \mathbf{M} \tag{11}$$

Thus,

$$\mathbf{IR}(p,q) = \mathrm{IRT}(\mathbf{S}(t,f), \boldsymbol{\theta}_{set} n^{opt}) = \mathrm{IRT}(\mathbf{S}(t,f), \boldsymbol{\alpha}^{opt}) \tag{12}$$

The $D_\perp$ can be inferred by identifying two points (P_1;P_2) in the IRT domain.

Doing this operation we will refer to an index j that can assume two values, i.e., j=1,2. With j=1 we identify the point P_1 having maximum distance from O, (k_1, m_1) are the coordinates of the selected point.

The second point to be selected is the one that lays in the subset of the IRT domain delimited by a line l orthogonal to $\overline{OP_1}$. In order to estimate the maximum size of the OUT we need to find the point of the target that is diagonally opposite to P_1 . Our algorithm searches for the peak at maximum euclidean distance from O. Thus, in case of asymmetrical objects we need to exclude the side of the object where the first detection is located. Otherwise we would estimate the RSO size incorrectly. The segment $\overline{OP_1}$ can be regarded as the principal diagonal of the object (See Figure 4). This is achieved in practice by exploiting a geometrical mask, defined as follow:

$$\mathbf{MASK}(p,q) = \begin{cases} 0 & (p,q) \geq l \\ 1 & (p,q) \leq l \end{cases} \tag{13}$$

where l is a line defined as follow

$$l : l \perp \overline{OP_1} \tag{14}$$

As it can be noticed from Figure 3, this mask is used

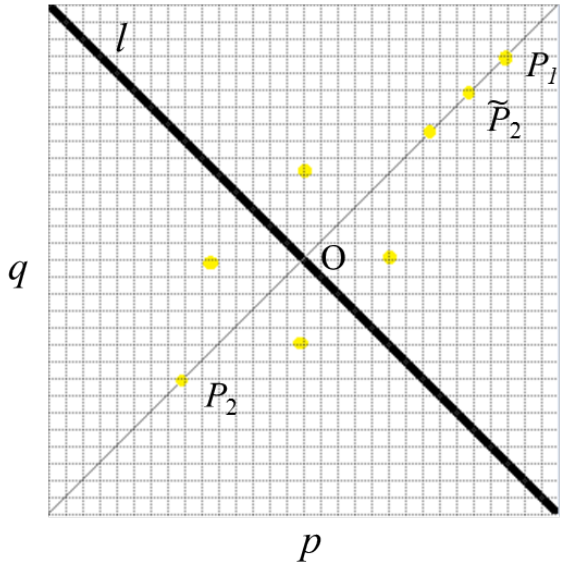

Figure 4: Geometry of reference for the mask definition

to define a subset of peaks over the IRT domain. This prevents the peak located in $\tilde{P}_2$ from being selected in place of the one located in P_2.

Once the selection is done, from the coordinates (k_j, m_j) of the selected points (SPs) we can estimate:

- The modulation amplitude as:

$$A_j = \left[\sqrt{k_j^2 + m_j^2}\right] \tag{15}$$

- The modulation phase as:

$$\phi_j = \arctan(m_j/k_j) \tag{16}$$

- The modulation frequency as:

$$\hat{f}_m = \frac{n^{opt}}{L} \tag{17}$$

Then, it is possible to write the corresponding sinusoid as follows:

$$a^{(j)}(t) = A_j \cos(2\pi \hat{f}_m t + \phi_j) \tag{18}$$

After a scaling transformation, we obtain the corresponding sinusoid in the spectrogram domain:

$$\hat{s}^{(j)}(t) = \hat{f}^{(j)}_{D_{max}} \cos\left(\frac{\hat{\Omega}}{f_s} t + \phi_j\right) \tag{19}$$

As mentioned above, from one Doppler signature we want to extract three characteristic parameters ($f_{D_{max}}$, $D_\perp$, T_Ω). In the following sections the relationships used to accomplish this task are given.

4.1. Estimation of T_Ω

Given the modulation frequency estimated from the Doppler signatures as in Equation 17, the rotation period can be expressed as:

$$\hat{T}_\Omega = \frac{2\pi}{\hat{\Omega}},\ \hat{\Omega} = \frac{2\pi \hat{f}_m}{f_s} \tag{20}$$

with $f_s = N/T_{ob}$ and N corresponding to the number of pulses.

4.2. Estimation of $f_{D_{max}}$

Using the modulation amplitude estimated as in Equation 15, the maximum Doppler frequency is calculated using the following relation:

$$\hat{f}^{(j)}_{D_{max}} = \mathbf{F}(A_j) \tag{21}$$

where $-1/(2\,T_r) \leq \mathbf{F}(A_j) \leq 1/(2\,T_r)$ and T_r is the Pulse Repetition Interval.

4.3. Estimation of $D_\perp$

Using Equations 21 and 20, the distance from O to the j-th SP can be written as

$$\hat{D}^{(j)}_\perp = \frac{c}{2f_0} \frac{\hat{f}^{(j)}_{D_{max}}}{\hat{\Omega}} \tag{22}$$

Thus, the estimation of the maximum size of the object is given by:

$$\hat{D}_\perp = \hat{D}^{(1)}_\perp + \hat{D}^{(2)}_\perp \tag{23}$$

5. PERFORMANCE ANALYSIS

5.1. Performance parameters

In this section, the performance indicators that have been used for the performance analysis are described.

1. **Mean Percentage Error**
   The *Mean Percentage Error* (%Err) is the mean value among the number of several realizations of noise (N_r). The %Err is defined as the magnitude of the difference between the exact value a and the estimation f_r divided by the magnitude of the exact value times 100 to express it in percent.

$$\%\text{Err} = \sum_{r=1}^{N_r} \left| \frac{a - f_r}{a} \right| \cdot 100 \tag{24}$$

2. **Normalized Root Mean Square Percentual Error**
   The *Root Mean Square Error* (RMSE) is frequently used as a measure of the difference between values (sample and population values) predicted by a model or an estimator and the values actually observed.

$$\text{RMSE} = \sqrt{\frac{1}{N_r} \sum_{r=1}^{N_r} (a - f_r)^2} \tag{25}$$

   Normalizing the RMSD facilitates the comparison between datasets or models with different scales.

$$\text{NRMSE} = \frac{RMSE}{a} \tag{26}$$

   The NRMSE expressed in percentual form gives the *Normalized Root Mean Square Percentual Error* (%NRMSE):

$$\%\text{NRMSE} = \text{NRMSE} \cdot 100 \tag{27}$$

5.2. Simulations set up

The parameters used to generate the simulated radar signal are shown in Table 1.

Simulated radar system		
Symbol	**Description**	**Value**
f_0	*Carrier frequency*	5 GHz
T_{ob}	*Observation Time*	1.4 s
f_s	*Sampling frequency*	13.2 kHz
T_r	*Pulse Repetition Interval*	75.7 μ s
T_i	*Pulse Width*	1.25 ns

Table 1: Simulated radar system parameters

To simplify the problem we modelled targets as a series of point scatterers. The point scatterer model is used under the assumption to observe objects having multiple-structures with size smaller than the sensor resolution.

This model, called the point scatterer model, is widely used in many radar application. In fact, the electromagnetic backscattered signal from a complex object can be thought as backscattering from a set of scattering centres on the object. As a result, the high resolution allows for such points to be mapped as point-scatterers. The point-scatterer model can be related to the electromagnetic scattering theory through high frequency ray optics where a set of highly localized ray phenomena can be related to a reflection or diffraction point on the object. These points can include specular reflections from smooth surfaces, edge diffractions from edge and tips, as well as multiple scattering from dihedral and trihedral corner reflections. An 8-objects database has been built as shown in Figure 5.

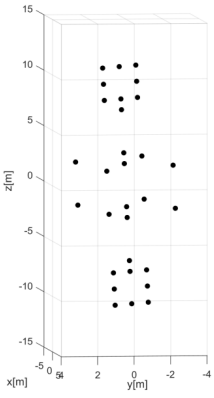

(a)

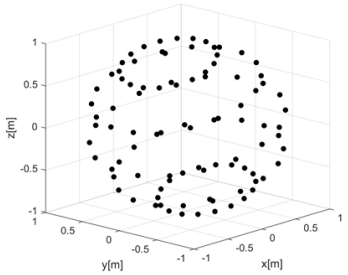

(b)

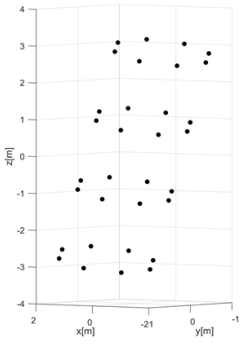

(c)

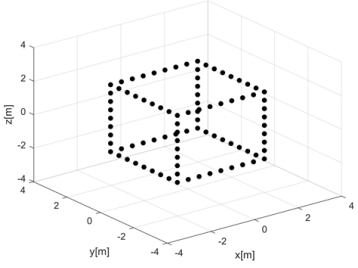

(d)

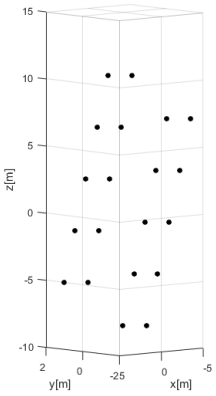

(e)

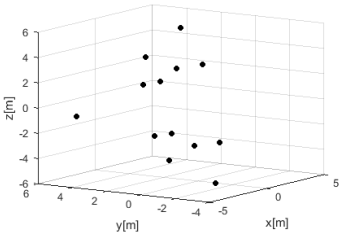

(f)

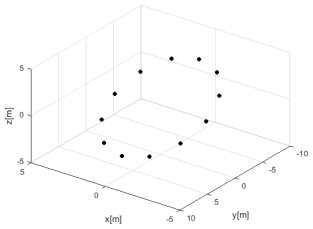

(g)

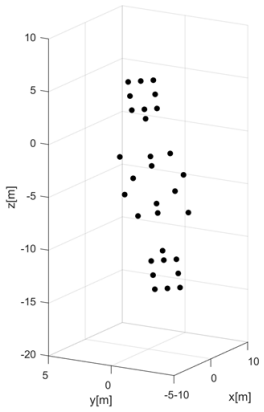

(h)

Figure 5: *RSO Database*.
(a) RSO 1: Satellite; (b) RSO 2: Sphere; (c) RSO 3: Cylinder; (d) RSO 4: Cube; (e) RSO 5: Parallelepiped; (f) RSO 6: Cone; (g) RSO 7: Disk; (h) RSO 8: Asymmetric Satellite.

The geometrical and dynamic properties used to create the RSO dataset are outlined in table 2 .

5.3. Results

The analysis of simulated data aims at testing the effectiveness of the proposed Feature Extraction Algorithm. To investigate the performances in low signal to noise ratio, complex white Gaussian noise is added to the simulated data in order to have a pre-selected SNR. In particular, the algorithm has been tested for four different values of SNR :{ -5, 0, 10, 20} dB. The performances analysis has been described in Sec. 5.1 in terms of Normalized Mean Percentage Error and Normalized Root Mean Square Percentage Error for the parameters $f_{D_{max}}$, $D_{\perp}$ and T_{Ω}.

The results obtained with a low SNR of -5 dB for RSO 1 and RSO 2 are shown in Figures 6 and 7, respectively. Even if the spectrograms in Figures 6b and 7b are very

RSO Dataset Geometrical and dynamic properties					
RSO	**Shape**	**Size** (x × y × z) [m]	$D_\perp$[m]	$f_{D_{max}}$[Hz]	T_Ω[s]
1	Satellite	4 × 4 × 22	22.0907	6614.1043	0.3500
2	Sphere	2 × 2 × 2	2	449.1096	0.4667
3	Cylinder	2 × 2 × 6	6.3246	2840.4188	0.2333
4	Cube	4 × 4 × 4	5.6569	1270.2739	0.4667
5	Parallelepiped	2 × 16 × 4	18.5536	5369.0052	0.4000
6	Cone	12 × 6 × 12	12	2245.5482	0.5600
7	Disk	12 × 12 × 0	12	4491.0965	0.2800
8	Asym Satellite	4 × 4 × 22	22.114	4799.8502	0.7000

Note: The distance between the radar and each RSO is R_0=900 Km

Table 2: RSO Dataset Geometrical and dynamic properties

noisy. We can conclude that good results can still be obtained by applying the proposed algorithm as shown in Figures 6d-6e and Figures 7d-7e.

It should be pointed out that thresholds are not optimal for any object in the database. Having to deal with highly different objects in term of shape, size and spin an absolutely optimal threshold cannot be found. Since, an optimal threshold is not the matter of the proposed technique a threshold high enough to suppress the majority of noise and low enough to retain the useful signal, has been heuristically selected.

The performance parameters obtained for each object in the database with SNR :{ -5, 0, 10, 20} dB are listed in Tables 3-10.

As shown in Tables 3-10 the estimation performances strictly depend from the value of $f_{D_{max}}$. Objects with higher $f_{D_{max}}$ show better performances then the others. This quantity, and thus its estimate, is a function of T_Ω, $f_{D_{max}}$ and f_0. Further study on their variation effect on the estimation performances are interest of the authors.

RSO 1				
		T_Ω	$f_{D_{max}}$	$D_\perp$
SNR=-5dB	%Err	0,353	0,084	0,506
	%NRMSE	0,382	0,084	0,527
SNR=0dB	%Err	0,190	0,084	0,344
	%NRMSE	0,195	0,084	0,346
SNR=10dB	%Err	0,087	0,084	0,240
	%NRMSE	0,088	0,084	0,241
SNR=20dB	%Err	0,093	0,084	0,246
	%NRMSE	0,093	0,084	0,246

Table 3: RSO 1 performance parameters

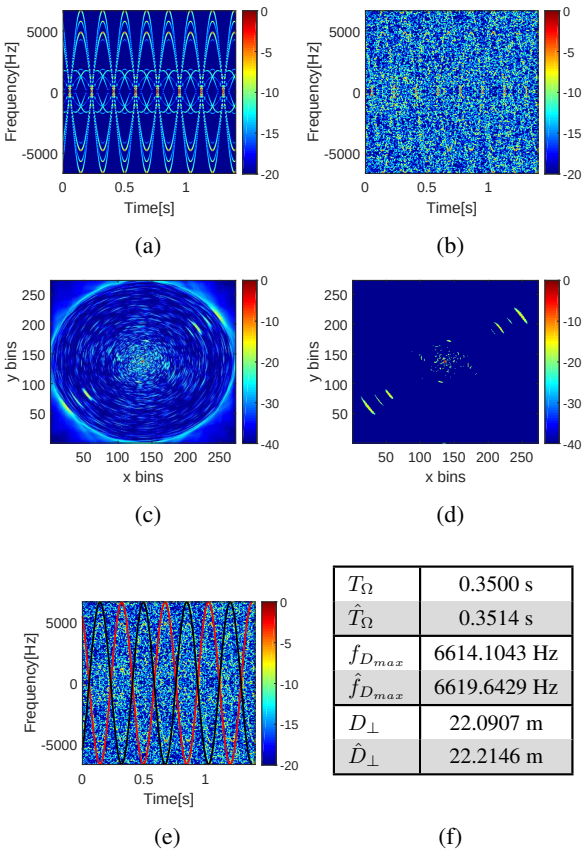

T_Ω	0.3500 s
$\hat{T}_\Omega$	0.3514 s
$f_{D_{max}}$	6614.1043 Hz
$\hat{f}_{D_{max}}$	6619.6429 Hz
$D_\perp$	22.0907 m
$\hat{D}_\perp$	22.2146 m

(f)

Figure 6: *Feature Extraction Algorithm Outputs for* RSO 1.
(a) spectrogram without noise;
(b) spectrogram with SNR= -5 dB;
(c) Inverse Radon Transform (IRT) with SNR= -5 dB;
(d) IRT with SNR= -5 dB after threshold;
(e) Reconstructed edge signatures;
(f) Estimated features.

RSO 2				
		T_Ω	$f_{D_{max}}$	$D_\perp$
SNR=-5dB	%Err	0,670	6,385	5,315
	%NRMSE	0,697	8,039	6,907
SNR=0dB	%Err	0,717	3,775	3,101
	%NRMSE	0,724	4,335	3,747
SNR=10dB	%Err	0,710	3,340	2,677
	%NRMSE	0,711	3,340	2,677
SNR=20dB	%Err	0,714	3,340	2,672
	%NRMSE	0,714	3,340	2,672

Table 4: RSO 2 performance parameters

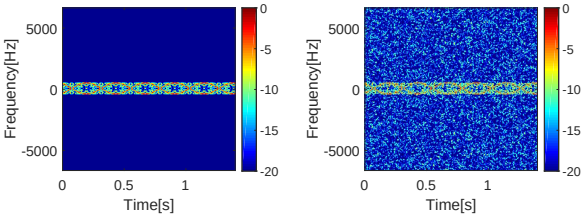

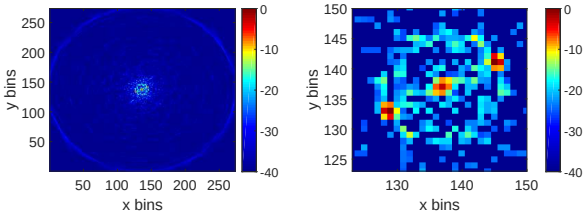

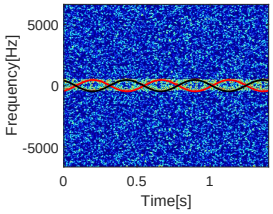

T_Ω	0.46667 s
$\hat{T}_\Omega$	0.46336 s
$f_{D_{max}}$	449.1096 Hz
$\hat{f}_{D_{max}}$	464.1078 Hz
$D_\perp$	2 m
$\hat{D}_\perp$	2.0536 m

(f)

Figure 7: *Feature Extraction Algorithm Outputs for* RSO 2.
(a) spectrogram without noise;
(b) spectrogram with SNR= -5 dB;
(c) Inverse Radon Transform (IRT) with SNR= -5 dB;
(d) IRT with SNR= -5 dB after threshold;
(e) Reconstructed edge signatures;
(f) Estimated features.

RSO 3				
		T_Ω	$f_{D_{max}}$	$D_\perp$
SNR=-5dB	%Err	0,096	41,832	48,575
	%NRMSE	0,107	49,986	52,747
SNR=0dB	%Err	0,039	1,104	1,018
	%NRMSE	0,046	1,104	1,019
SNR=10dB	%Err	0,035	1,104	1,003
	%NRMSE	0,041	1,104	1,003
SNR=20dB	%Err	0,038	1,104	0,998
	%NRMSE	0,038	1,104	0,998

Table 5: RSO 3 performance parameters

RSO 4				
		T_Ω	$f_{D_{max}}$	$D_\perp$
SNR=-5dB	%Err	0,144	1,916	1,840
	%NRMSE	0,151	1,916	1,840
SNR=0dB	%Err	0,121	1,916	1,864
	%NRMSE	0,122	1,916	1,864
SNR=10dB	%Err	0,169	1,916	1,815
	%NRMSE	0,169	1,916	1,815
SNR=20dB	%Err	0,172	1,916	1,811
	%NRMSE	0,172	1,916	1,811

Table 6: RSO 4 performance parameters

RSO 5				
		T_Ω	$f_{D_{max}}$	$D_\perp$
SNR=-5dB	%Err	0,055	0,364	0,422
	%NRMSE	0,063	0,364	0,440
SNR=0dB	%Err	0,026	0,364	0,454
	%NRMSE	0,032	0,364	0,454
SNR=10dB	%Err	0,036	0,364	0,464
	%NRMSE	0,038	0,364	0,464
SNR=20dB	%Err	0,031	0,364	0,460
	%NRMSE	0,031	0,364	0,460

Table 7: RSO 5 performance parameters

RSO 6				
		T_Ω	$f_{D_{max}}$	$D_\perp$
SNR=-5dB	%Err	0,550	1,251	0,721
	%NRMSE	0,562	1,322	0,769
SNR=0dB	%Err	0,197	1,773	1,643
	%NRMSE	0,202	2,024	1,913
SNR=10dB	%Err	0,229	1,164	1,002
	%NRMSE	0,230	1,164	1,002
SNR=20dB	%Err	0,264	1,164	0,967
	%NRMSE	0,264	1,164	0,967

Table 8: RSO 6 performance parameters

RSO 7				
		T_Ω	$f_{D_{max}}$	$D_\perp$
SNR=-5dB	%Err	0,067	20,265	26,934
	%NRMSE	0,079	22,509	28,476
SNR=0dB	%Err	0,107	0,535	1,004
	%NRMSE	0,116	0,540	1,774
SNR=10dB	%Err	0,198	0,620	0,398
	%NRMSE	0,200	0,620	0,436
SNR=20dB	%Err	0,251	0,620	0,437
	%NRMSE	0,251	0,620	0,437

Table 9: RSO 7 performance parameters

RSO 8				
		T_Ω	$f_{D_{max}}$	$D_\perp$
SNR=-5dB	%Err	0,666	0,254	0,323
	%NRMSE	0,691	0,254	0,360
SNR=0dB	%Err	0,571	0,254	0,187
	%NRMSE	0,578	0,254	0,231
SNR=10dB	%Err	0,698	0,254	0,284
	%NRMSE	0,699	0,254	0,286
SNR=20dB	%Err	0,726	0,254	0,312
	%NRMSE	0,726	0,254	0,313

Table 10: RSO 8 performance parameters

6. CONCLUSIONS

Radar echoes from space debris typically have highly non-stationary Doppler due to their dynamics (spin). According to the derived signal model, this paper has proposed a novel method for RSO feature estimation. The proposed method is based on the use of the spectrogram and the IRT. The influence of noise on the estimation procedure has also been considered. The proposed method has shown good accuracy and robustness with respect to noise.

ACKNOWLEDGMENTS

This work has been supported by funds from the Air Force Research Lab (AFRL) under the EOARD Project - FA9550-14-1-0183.

REFERENCES

1. Klinkrad H., (2006). Space Debris -Models and Risk Analysis-. *Encyclopedia of Aerospace Engineering*, Wiley.

2. Klinkrad H., (2010). Space Debris -Environmental Impact, Manufacturing and Operations-. *Springer Berlin Heidelberg*.

3. Clissold P., (2009). Space Debris.*ESA Communication Production Office*, BR-274.

4. National Research Council, (2012). Continuing Kepler's Quest -Assessing Air Force Command's Astrodynamics Standards-.*The National Academies Press*.

5. (2012). Continuing Kepler's Quest -Assessing Air Force Command's Astrodynamics Standards. *National research Council, The National Academic Press*.

6. Chen V.C. ,Li F.,Ho S.-S.,Wechsler H., (2006). Micro-Doppler effect in radar: phenomenon, model, and simulation study.*IEEE Transactions on Aerospace and Electronic Systems*, **42**, 2–21.

7. Sato T., (1999). Shape Estimation of Space Debris Using Single-Range Doppler Interferometry. *IEEE Transactions on Geoscience and Remote Sensing*, **37**, 2.

8. Zhang L., Li Y. C.,Liu Y., et al., (2010). Time-frequency characteristics based motion estimation and imaging for high speed spinning targets via narrowband waveforms. *Science China: Information Sciences*, **53**, 1628-1640.

9. Li J., Qiu C. W., Zhang L., et al., (2010). Time-frequency imaging algorithm for high speed spinning targets in two dimensions. *IET Radar, Sonar and Navigation*, **4**, 806-817.

10. Chen V., (2011).The micro-Doppler effect in radar, Artech House.

11. Stankovic L.,(2003). Measuring Time-Frequency distributions concentration, in *Time-Frequency Signal Analysis and Processing*, Elsevier, 1820—1825.